Simultaneous Antiferromagnetic Order and Spin-Glass-like Behavior in $MnAsO_4$

Miguel A. G. Aranda,*,† J. Paul Attfield,‡ Elaine Batchelor,‡ Greg P. Shields,‡ Sebastián Bruque,† and Mercedes Gabás§

Departamento de Química Inorgánica, Cristalografía y Mineralogía, Universidad de Málaga, 29071 Málaga, Spain, Department of Chemistry, University of Cambridge, Lensfield Road, Cambridge CB2 1EW, U.K., and Departamento de Física Aplicada, Universidad de Málaga, 29071 Málaga, Spain

Received July 15, 1997

A low-temperature time-of-flight neutron powder diffraction study of a simple new solid, $MnAsO_4$, in a sample also containing 20% $Mn_2As_2O_7$ has been performed. $MnAsO_4$ orders magnetically at 14.5(5) K, and the unusual antiferromagnetic structure below this temperature has been determined. Only half of the Mn^{3+} spins are ordered, and the remaining "idle" spins show some spin-glass behavior evidenced by susceptibility measurements. The ordered moment is reduced to a value of 2.6 μ_B by frustration. It is not possible to determine which of the two crystallographically inequivalent Mn sublattices is magnetically ordered and which is idle. The antiferromagnetic structure of the minority phase $Mn_2As_2O_7$ which orders at 10.5(5) K has also been determined.

Introduction

Anhydrous transition metal oxo salts exhibit a great variety of magnetic properties due in part to the different crystal structures that may be adopted. One structure commonly found in many MXO_4 compounds, where M is a transition metal ion and XO_4 a tetrahedral anion, is the $CuSO_4$ type structure.[1,2] These compounds have a primitive orthorhombic unit cell (space group *Pmnb*, $a \approx 7.0$ Å, $b \approx 8.5$ Å, and $c \approx 5.0$ Å). The structure consists of infinite chains of trans-edge-sharing MO_6 octahedra running parallel to [100] that are linked by the XO_4 tetrahedral groups to give a three-dimensional framework. There is only one independent crystallographic site for the metal cation, and for M = Cu^{2+}, the oxygen environment shows a typical [4+2] Jahn−Teller distortion with two long Cu−O bonds. Magnetic superexchange within and between spin chains leads to long-range magnetic ordering which has been detected using neutron diffraction in many salts with this structure type, e.g, $CuSO_4$,[3] $CuSeO_4$,[4] and $MnSeO_4$.[5]

We recently synthesized the previously unknown phase $MnAsO_4$ as an intermediate thermal decomposition product of $MnAsO_4{\cdot}H_2O$, although it is always contaminated with the final decomposition product, $Mn_2As_2O_7$.[6] Structure refinement using powder X-ray diffraction data shows $MnAsO_4$ to be a unique example of a monoclinically distorted $CuSO_4$ type structure. The chains of edge-sharing MnO_6 octahedra contain two alternating Mn^{3+} sites that display cooperative [4+2] and [2+2+2] Jahn−Teller distortions. It was previously suggested that the cooperative distortion might result in a ferromagnetic spin−spin coupling within the chains.[6] We have subsequently determined the magnetic structure of this compound and the $Mn_2As_2O_7$ secondary phase using low-temperature time-of-flight powder neutron diffraction, which we used previously to determine the magnetic structures of $MnXO_4{\cdot}D_2O$ (X = As, P)[7] and the ion-exchanged derivatives $LiMnXO_4(OD)$ (X = As,[8] P[9]), giving the results presented here.

Experimental Section

$MnAsO_4$ was synthesized by thermal decomposition of $MnAsO_4{\cdot}H_2O$ at 325 °C as previously described,[6] which gives a minimum (20%) contamination of the pyroarsenate $Mn_2As_2O_7$. A single-phase sample of $Mn_2As_2O_7$ was also synthesized by heating $MnAsO_4{\cdot}H_2O$ at 800 °C.[10]

Molar magnetic susceptibility measurements were performed on the $MnAsO_4/Mn_2As_2O_7$ and pure $Mn_2As_2O_7$ samples, and subtraction of 22% (determined by Rietveld X-ray analysis of the two-phase sample) of the latter curve from the former was used to estimate the susceptibility of $MnAsO_4$. Dc and ac susceptibilities were measured on Quantum Design MPMS SQUID magnetometers. Dc susceptibilities were measured between 5 and 250 K at 100 Oe applied field. Subsequent field-cooled and zero-field-cooled data were recorded on a different instrument in fields of 10, 50, and 100 Oe (the residual magnetic field had an estimated value of 0.01−0.1 Oe). Low-temperature ac magnetization measurements were performed at frequencies of 1 and 10 Hz in an excitation field of 4.5 Oe.

Time-of-flight neutron powder diffraction patterns from a 10 g $MnAsO_4/Mn_2As_2O_7$ sample were collected on the high-intensity powder diffractometer (HIPD) at MLNSC, Los Alamos National Laboratory, at 15 and 11 K. Six spectra were recorded at each temperature by counters at 2θ angles ±40, ±90, and ±150° covering *d*-space ranges

* To whom the correspondence should be addressed. E-mail: g_aranda@uma.es.

† Departamento de Química Inorgánica, Cristalografía y Mineralogía, Universidad de Málaga.

‡ University of Cambridge.

§ Departamento de Física Aplicada, Universidad de Málaga.

(1) Kokkoros, P. A.; Rentzeperis, P. J. *Acta Crystallogr.* **1958**, *11*, 361.
(2) Wildner, M.; Giester, G. *Miner. Petrol.* **1988**, *39*, 201.
(3) Almodovar, I.; Frazer, B. C.; Hurst, J. J.; Cox, D. E.; Brown, P. J. *Phys. Rev* **1965**, *129*, A153.
(4) Scharenberg, W.; Will, G. *J. Phys. C1* **1971**, *32*, 851.
(5) Fuess, H.; Will, G. *J. Appl. Phys.* **1968**, *39*, 628.
(6) Aranda, M. A. G.; Attfield, J. P.; Bruque, S. *Inorg. Chem.* **1993**, *32*, 1925.
(7) Aranda, M. A. G.; Attfield, J. P.; Bruque, S.; Palacio, F. *J. Mater. Chem.* **1992**, *2*, 501.
(8) Aranda, M. A. G.; Attfield, J. P.; Bruque, S.; Von Dreele, R. B. *J. Chem. Soc., Chem. Commun.* **1994**, 155.
(9) Aranda, M. A. G.; Bruque, S.; Attfield, J. P.; Palacio, F.; Von Dreele, R. B. *J. Solid State Chem.* **1997**, *132*, 202.
(10) Aranda, M. A. G.; Bruque, S.; Attfield, J. P. *Inorg. Chem.* **1991**, *30*, 2043.

S0020-1669(97)00858-6 CCC: $15.00
Published on Web 02/27/1998

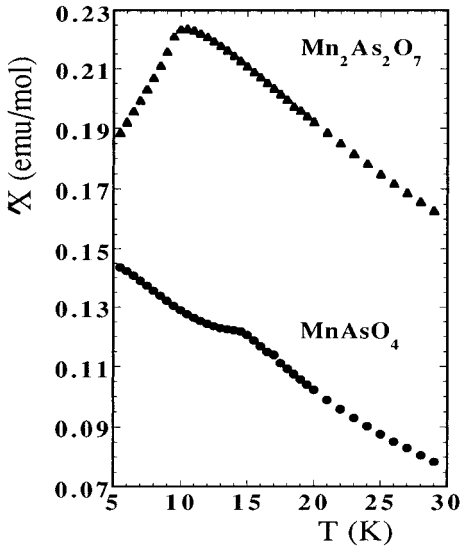

Figure 1. Molar magnetic susceptibility data for $MnAsO_4$ and $Mn_2As_2O_7$ between 5 and 30 K.

Table 1. Magnetic Susceptibility Results for $MnAsO_4$ and $Mn_2As_2O_7$

			μ_{eff}/μ_B	
	T_{max}/K	Θ/K	obsd	calcd
$Mn^{III}AsO_4$	14.5(5)	−8.6	5.1	4.9
$Mn^{II}{}_2As_2O_7$	10.5(5)	−3.9	5.6	5.9

of 1.40−8.39, 0.69−3.87, and 0.50−3.78 Å, respectively. Further data were collected on the high-resolution powder diffractometer (HRPD) at Rutherford Appleton Laboratory, U.K., at 5 and 1.6 K. This diffractometer is optimized for very high resolution with detector banks at 90 and 170° covering *d* spacings ranging 0.69−3.87 and 0.50−3.78 Å, respectively.

All the time-of-flight data were normalized to the incident-beam spectrum and fitted by the Rietveld method[11,12] using the GSAS package.[13] This enables the contributions of several crystal and magnetic structures to be fitted to the data simultanously. A standard Al_2O_3 neutron diffraction pattern recorded on the HRPD was used to calibrate the *d*-space scale. Simultaneous refinements of all the histograms for a given temperature were performed with (i) a Gaussian convoluted with a double-exponential peak shape function[14] and (ii) a refined Fourier series background function. Neutron scattering lengths were taken from Koster and Yelon,[15] and the free Mn ion magnetic form factor of Freeman and Watson[16] was used to calculate the magnetic intensities. The fits to individual profiles gave values of R_{WP} between 2.0% and 3.0%.

Results

The low-temperature molar susceptibilities of $MnAsO_4$ and $Mn_2As_2O_7$ are displayed in Figure 1. The high-temperature susceptibility data for both compounds were fitted by Curie−Weiss curves, after diamagnetic corrections,[17] and the derived parameters are given in Table 1. Both $MnAsO_4$ and $Mn_2As_2O_7$ order magnetically at low temperatures (Figure 1). The maximum in the curve for $Mn_2As_2O_7$ signifies a typical antiferromagnetic transition at 10.5(5) K. However, the low-temperature data for $MnAsO_4$ do not show a normal behavior below the magnetic transition temperature at 14.5(5) K.

Table 2. Refined Components and Resultant Values of the Magnetic Moments for $MnAsO_4$ and $Mn_2As_2O_7$ as Functions of Temperature[a]

	T/K	μ_x/μ_B	μ_z/μ_B	μ_R/μ_B
$MnAsO_4$	11	1.35(1)	−1.39(3)	1.93(2)
	5	1.06(13)	−2.17(10)	2.42(10)
	1.6	1.05(7)	−2.32(5)	2.55(5)
$Mn_2As_2O_7$	5	−0.08(35)	3.45(15)	3.45(15)
	1.6	1.14(18)	4.08(7)	4.24(4)

[a] The magnetic moments lie in the *ac* plane.

To study the magnetic ordering behavior of these phases, powder neutron diffraction data from the $MnAsO_4/Mn_2As_2O_7$ sample were collected above both transitions at 15 K; at 11 K, where only $MnAsO_4$ is magnetically ordered; and at 5 and 1.6 K (the lowest accessible temperature), where both $MnAsO_4$ and $Mn_2As_2O_7$ should be ordered. No unexpected structural changes take place for either phase on cooling from room temperature to 15 K, and the data (Figure 2a) could be fitted satisfactorily using the room-temperature crystal structures of $MnAsO_4$[6] and $Mn_2As_2O_7$[10] as starting models. The molar composition of the mixture was determined from the refined phase scale factors to be 80.8(7)% for $MnAsO_4$ and 19.2(7)% for $MnAsO_{3.5}$ ($=1/2$ $Mn_2As_2O_7$).

Magnetic diffraction peaks were clearly observed in the 11 K neutron patterns (Figure 2b). These peaks could be indexed on the structural unit cell of $MnAsO_4$ by doubling the *a* and *c* parameters. No magnetic ordering of $Mn_2As_2O_7$ was detected, in agreement with the susceptibility results. The $MnAsO_4$ magnetic peaks have *hkl* conditions *h* odd, *l* odd, and the same parity for $(h + l)/2$ and *k*, and magnetic models consistent with these conditions were tested by fits to the data. There are 16 Mn atoms in the $2a \times b \times 2c$ magnetic supercell derived from the two crystallographically independent Mn positions in the fundamental structural cell. It was not possible to fit the magnetic intensities with magnetic moments at all the sites derived from the Mn(a) and Mn(b) positions. However, an excellent fit was obtained with the collinear magnetic moments placed only at the 8 Mn(a) positions in the magnetic supercell with the following relative spin directions: (0, 0, 0) +; ($1/2$, 0, 0) −; (0, 0, $1/2$) −; ($1/2$, 0, $1/2$) +; ($1/4$, $1/2$, $1/4$) +; ($3/4$, $1/2$, $1/4$) −; ($1/4$, $1/2$, $3/4$) −; ($3/4$, $1/2$, $3/4$) +. It is notable that as Mn(a) and Mn(b) are related by a simple translational operation of $\pm a/2$, an entirely equivalent magnetic fit can be obtained by placing the moments on the positions derived from Mn(b) and leaving the Mn(a) sites without spin density. The magnetic moment was found to lie in the *ac* plane, and the refined component values are given in Table 2.

Analysis of the 5 and 1.6 K data shows that no transition to a fully ordered magnetic structure takes place for $MnAsO_4$. New peaks were observed (see Figure 3) which could not be indexed on the $MnAsO_4$ cell but could be indexed upon an $a \times b \times 2c$ supercell of the monoclinic $Mn_2As_2O_7$ structure. The reflection conditions of the magnetic peaks for the $Mn_2As_2O_7$ were $(h + k + l)$ odd referred to the magnetic cell. There is one crystallographically independent Mn atom in the structural unit cell which generates eight Mn positions in the magnetic supercell. A good fit to the magnetic intensities was obtained with a collinear model with moments lying in the *ac* plane (see Figure 3 and Table 2). The relative spin directions in the $a \times b \times 2c$ magnetic supercell were as follows: (0, 0.31, $1/4$) +;

(11) Rietveld, H. M. *J. Appl. Crystallogr.*, **1969**, 2, 65.
(12) Young, R. A., Ed. *The Rietveld Method*; Oxford University Press: Oxford, U.K., 1993.
(13) Larson, A. C.; Von Dreele, R. B. Report LA-UR-86-748; Los Alamos National Laboratory: Los Alamos, NM, 1994.
(14) Von Dreele, R. B.; Jorgensen J. D.; Windsor, C. G. *J. Appl. Crystallogr.*, **1982**, *15*, 581.
(15) Koster, L.; Yelon, W. B. *Summary of low energy neutron scattering wavelengths and cross sections*; Netherland Energy Research Foundation: Petten, The Netherlands, 1982.
(16) Freeman, A. J.; Watson, R. E. *Acta Crystallogr.* **1961**, *14*, 231.
(17) O'Connor, C. J. *Prog. Inorg. Chem.* **1982**, *29*, 203.

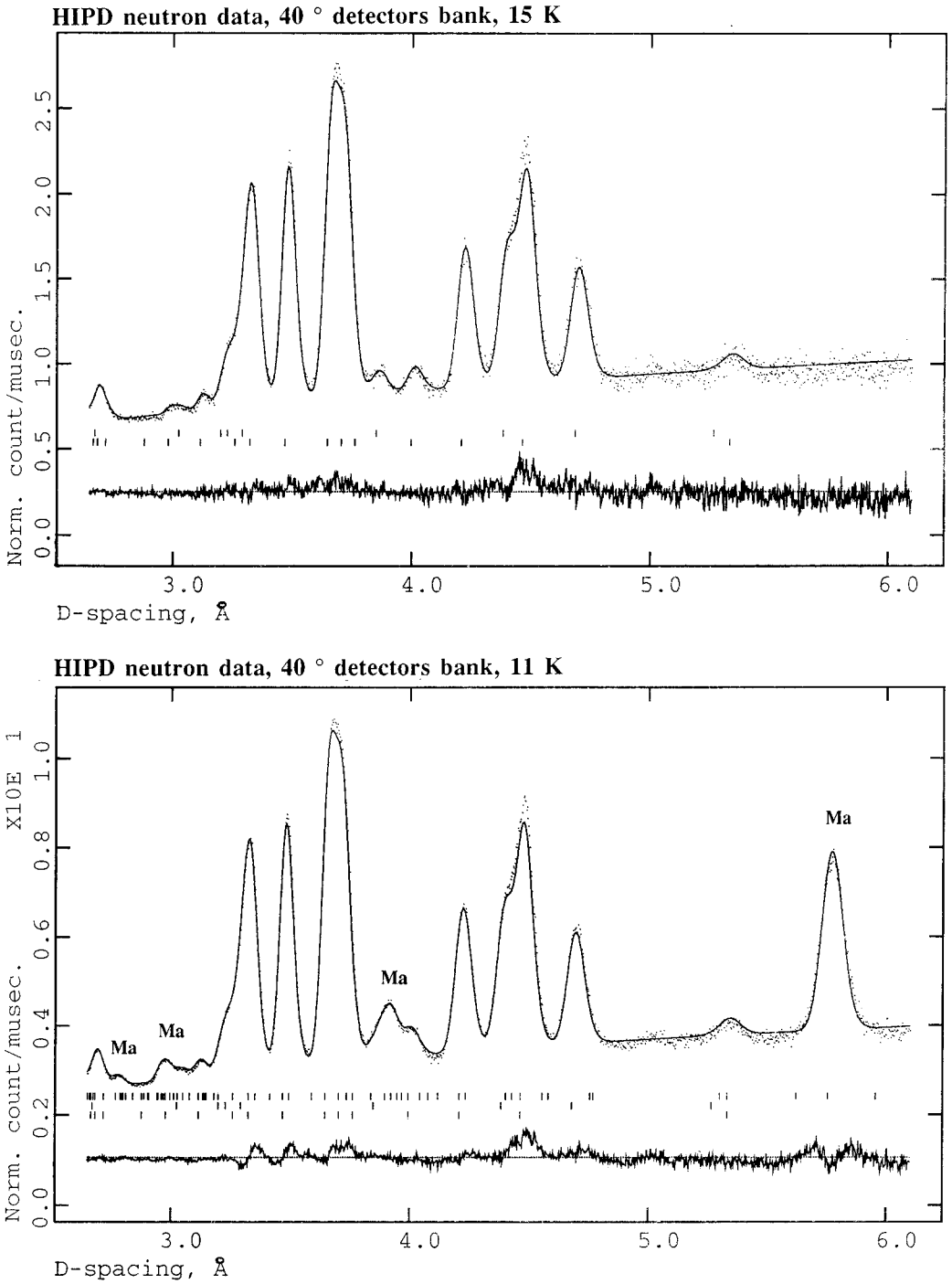

Figure 2. Final observed (points), calculated (full line), and difference HIPD pulsed neutron powder diffraction patterns (40° detector) at (a) 15 K and (b) 11 K. Markers are shown for $MnAsO_4$ (lower) and $Mn_2As_2O_7$ (upper). For the 11 K pattern, the upper row of markers corresponds to the magnetic supercell of $MnAsO_4$, and the more intense magnetic peaks are labeled as Ma.

($^1/_2$, 0.81, $^1/_4$) +; (0, 0.31, $^3/_4$) −; ($^1/_2$, 0.81, $^3/_4$) −; (0, 0.69, $^1/_4$) −; ($^1/_2$, 0.19, $^1/_4$) −; (0, 0.69, $^3/_4$) +; ($^1/_2$, 0.19, $^3/_4$) +.

Refined unit cell parameters for $MnAsO_4$ and $Mn_2As_2O_7$ at different temperatures are given in Table 3. Data ranges and agreement factors for the refinements of the HIPD and HRPD neutron diffraction data are given in the Supporting Information (Tables S1 and S2, respectively). Refined atomic parameters for $MnAsO_4$ and $Mn_2As_2O_7$ at 15 K are displayed in Tables 4 and 5, respectively. The atomic parameters for the other temperatures have been deposited as Supporting Information. Bond distances and angles for $MnAsO_4$ at 15 K are given in Table 6. The variation of bond distances with temperature for $MnAsO_4$ are shown in Table 7. Observed, calculated, and difference HIPD neutron powder diffraction patterns (40° detector) at 15 and 11 K are shown in Figure 2, parts a and b, respectively. A Rietveld plot of the HRPD neutron pattern at 1.6 K is displayed in Figure 3. Other results from the refinements, including the refined atomic parameters for $MnAsO_4$ and $Mn_2As_2O_7$, at all temperatures are given as Supporting Information in Tables S3−S9. The variation of the refined resultant magnetic moment of $MnAsO_4$ with temperature is given in Figure 4. A fit of the equation $M(T) = M_s(1 - T/T_N)^n$ gave a saturation magnetic moment of $M_s = 2.62\ \mu_B$ and the exponent $n = 0.20$.

The neutron diffraction study shows that half the Mn^{3+} spins in $MnAsO_4$ are not long range ordered below the antiferromag-

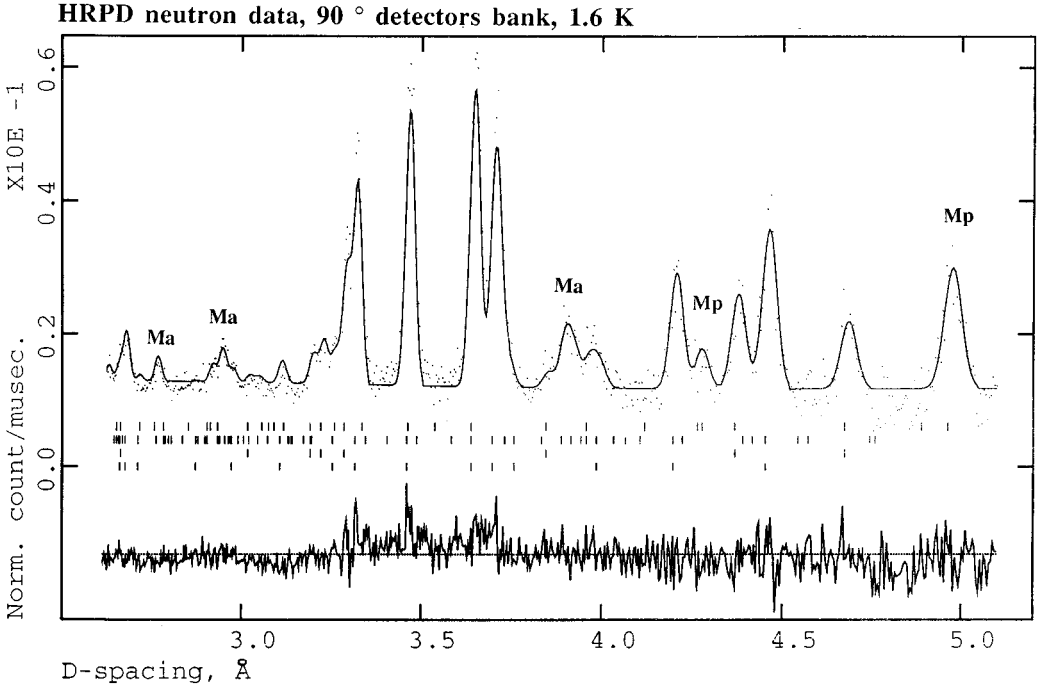

Figure 3. Rietveld plot for the HRPD pattern (90 ° detector) at 1.6 K, as in Figure 2. Prominent magnetic peaks are labeled Ma for $MnAsO_4$ and Mp for $Mn_2As_2O_7$.

Table 3. Variation of the Unit Cell Parameters with Temperature for $MnAsO_4$ and $Mn_2As_2O_7$

T/K	*a*/Å	*b*/Å	*c*/Å	*β*/deg
		$MnAsO_4$		
300[a]	6.6833(2)	8.9303(2)	4.7914(1)	93.813(2)
15	6.6627(1)	8.9346(1)	4.7838(1)	93.629(1)
11	6.6611(1)	8.9333(1)	4.7829(1)	93.625(1)
5	6.6576(5)	8.9293(6)	4.7815(2)	93.627(3)
1.6	6.6555(1)	8.9275(3)	4.7794(1)	93.617(2)
		$Mn_2As_2O_7$		
300[a]	6.7563(1)	8.7693(1)	4.8047(1)	102.831(1)
15	6.7539(3)	8.7713(5)	4.8018(1)	102.689(4)
11	6.7540(3)	8.7684(4)	4.8006(2)	102.702(4)
5	6.7503(9)	8.7576(15)	4.8018(10)	102.696(5)
1.6	6.7467(5)	8.7575(7)	4.8013(5)	102.706(6)

[a] Powder X-ray data taken from ref 6 for $MnAsO_4$ and from ref 10 for $Mn_2As_2O_7$.

Table 4. Refined Atomic Parameters for $MnAsO_4$ in the $P2_1/n$ Space Group, at 15 K, with Esd's in Parentheses

atom	sym pos	*x*	*y*	*z*	U_{iso}/Å^2
Mn(a)	2a	0	0	0	0.0046(2)
Mn(b)	2d	0.5	0.	0	0.0046
As	4e	0.2799(1)	0.1800(1)	0.4657(2)	0.0007(1)
O(1)	4e	0.2830(1)	0.1218(1)	0.7999(2)	0.0075(2)
O(2)	4e	0.7731(1)	0.1302(1)	0.9166(2)	0.0090(2)
O(3a)	4e	0.0629(1)	0.1219(1)	0.3113(2)	0.0064(2)
O(3b)	4e	0.4869(1)	0.1222(1)	0.3150(2)	0.0064(2)

netic transition temperature, 14.5 K. To tell whether these spins are still paramagnetic or randomly frozen in a glassy-like spin state, further dc and ac magnetization measurements were carried out. The dc data in Figure 5 comparing field cooled and zero-field-cooled magnetizations for a field of 100 Oe show a clear divergence below the ordering temperature of 14.5 K. This separation is much smaller at 50 Oe and barely detectable at 10 Oe. This behavior is consistent with spin-glass behavior below the magnetic transition. However, no anomaly in the imaginary part of the ac susceptibility (Figure 6), χ'', is seen at the transition, nor is there a difference between the data recorded at 1 and 10 Hz, which would also have been expected for normal spin-glass behavior. There is also an anomaly at 4.5 K in the real component of the ac susceptibility data, χ', the origin of which is not clear.

Table 5. Refined Atomic Parameters for $Mn_2As_2O_7$ in Space Group *C*2/*m* at 15 K

atom	sym pos	*x*	*y*	*z*	U_{iso}/Å^2
Mn	4h	0	0.3028(5)	0.5	0.009(1)
As	4i	0.2286(4)	0	−0.0945(6)	0.013(1)
O(1)[a]	4g	0	0.0368(6)	0	0.003(1)
O(2)	4i	0.3936(4)	0.00	0.2222(6)	0.003(1)
O(3)	8j	0.2356(3)	0.1586(2)	0.7182(4)	0.003(1)

[a] The occupation factor of O(1) was set to 0.5 to allow for disorder.

Table 6. Bond Distances (Å) and Angles (deg) for $MnAsO_4$ at 15 K

	MnO_6 Octahedra		
Mn(a)−O(1) × 2	2.426(1)	Mn(b)−O(1) × 2	2.004(1)
Mn(a)−O(2) × 2	1.929(1)	Mn(b)−O(2) × 2	2.217(1)
Mn(a)−O(3a) × 2	1.871(1)	Mn(b)−O(3b) × 2	1.868(1)
O(1)−Mn(a)−O(1)	180.0	O(1)−Mn(b)−O(1)	180.0
O(1)−Mn(a)−O(2) × 2	105.4(1)	O(1)−Mn(b)−O(2) × 2	101.8(1)
O(1)−Mn(a)−O(2) × 2	74.6(1)	O(1)−Mn(b)−O(2) × 2	78.2(1)
O(1)−Mn(a)−O(3a) × 2	85.0(1)	O(1)−Mn(b)−O(3b) × 2	89.9(1)
O(1)−Mn(a)−O(3a) × 2	95.0(1)	O(1)−Mn(b)−O(3b) × 2	90.1(1)
O(2)−Mn(a)−O(2)	180.0	O(2)−Mn(b)−O(2)	180.0
O(2)−Mn(a)−O(3a) × 2	93.1(1)	O(2)−Mn(b)−O(3b) × 2	85.4(1)
O(2)−Mn(a)−O(3a) × 2	86.9(1)	O(2)−Mn(b)−O(3b) × 2	96.4(1)
O(3a)−Mn(a)−O(3a)	180.0	O(3b)−Mn(b)−O(3b)	180.0
	AsO_4 Tetrahedron		
As−O(1)	1.681(1)	O(1)−As−O(2)	115.9(1)
As−O(2)	1.712(1)	O(1)−As−O(3a)	106.5(1)
As−O(3a)	1.665(1)	O(1)−As−O(3b)	110.6(1)
As−O(3b)	1.678(1)	O(2)−As−O(3a)	103.5(1)
		O(2)−As−O(3b)	105.2(1)
		O(3a)−As−O(3b)	115.3(1)
Mn(a)−O(1)−Mn(b)	97.1(1)	Mn(a)−O(2)−Mn(b)	106.7(1)
Mn(a)−O(1)−As	123.5(1)	Mn(a)−O(2)−As	123.7(1)
Mn(b)−O(1)−As	126.0(1)	Mn(b)−O(2)−As	120.7(1)
Mn(a)−O(3a)−As	132.8(1)	Mn(b)−O(3b)−As	127.5(1)

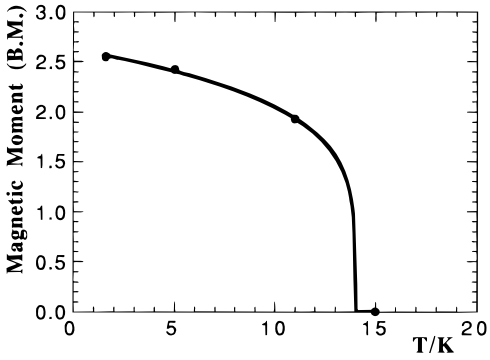

Figure 4. Variation of the refined resultant magnetic moment of $MnAsO_4$ with temperature. For details of the fit, see the text.

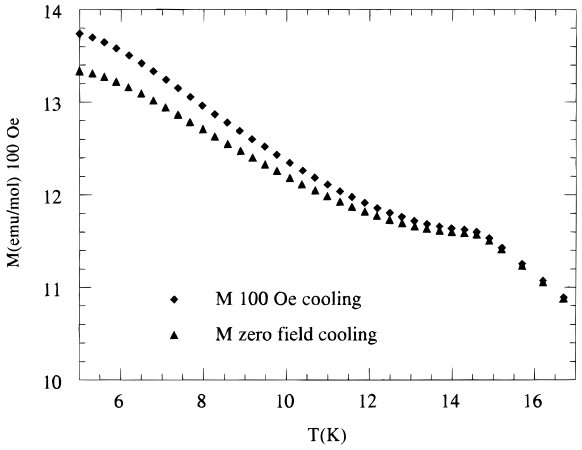

Figure 5. Field-cooling and zero-field-cooling magnetization data for $MnAsO_4$ between 5 and 17 K taken at an applied field of 100 Oe.

Table 7. Bond Distances (Å) for $MnAsO_4$ as a Function of Temperature

	15 K	11 K	5 K	1.6 K
Mn(a)−O(1) × 2	2.426(1)	2.425(1)	2.420(7)	2.412(3)
Mn(a)−O(2) × 2	1.929(1)	1.930(1)	1.936(7)	1.942(3)
Mn(a)−O(3a) × 2	1.871(1)	1.864(1)	1.895(7)	1.880(3)
Mn(b)−O(1) × 2	2.004(1)	2.000(1)	2.015(7)	1.999(3)
Mn(b)−O(2) × 2	2.217(1)	2.213(1)	2.198(6)	2.203(3)
Mn(b)−O(3b) × 2	1.868(1)	1.873(1)	1.861(8)	1.871(4)
As−O(1)	1.681(1)	1.686(1)	1.671(8)	1.686(4)
As−O(2)	1.712(1)	1.706(1)	1.734(9)	1.717(4)
As−O(3a)	1.665(1)	1.671(1)	1.624(8)	1.658(4)
As−O(3b)	1.678(1)	1.674(1)	1.672(7)	1.654(3)

Discussion

The 15 K crystal structures of $MnAsO_4$ and $Mn_2As_2O_7$ are similar to those previously determined at room temperature.[6,10] Only small differences due to thermal contraction are detected, and smooth variations in the cell parameters are observed between 15 and 1.6 K (see Table 3).

$MnAsO_4$. The high-temperature effective moment (Table 1) is typical for high-spin d^4 Mn^{3+}, and the negative Weiss Θ constant indicates that weak antiferromagnetic interactions occur between spins. No deviation from the Curie−Weiss law was observed between 30 and 200 K. However, the combination of neutron diffraction and magnetic measurements shows that a very unusual magnetic transition occurs at 14.5 K, below which one sublattice of Mn^{3+} spins orders antiferromagnetically while the other is disordered and behaves in some respects as a spin glass. A further unusual feature is that it is not possible to distinguish which Mn sublattice is magnetically ordered, as

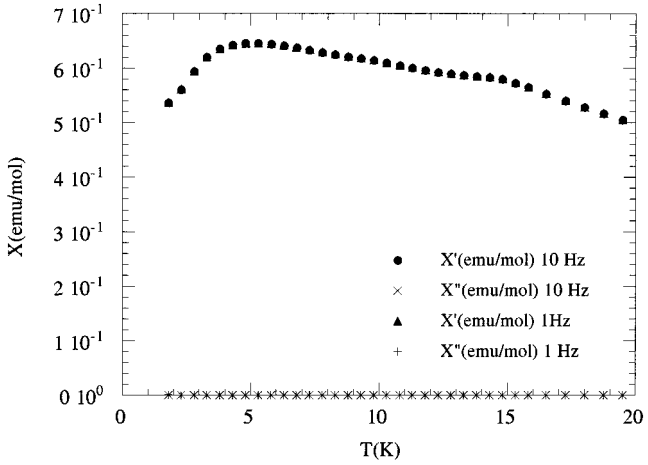

Figure 6. Ac susceptibility data showing real (χ') and imaginary (χ'') components for $MnAsO_4$ at frequencies of 1 and 10 Hz.

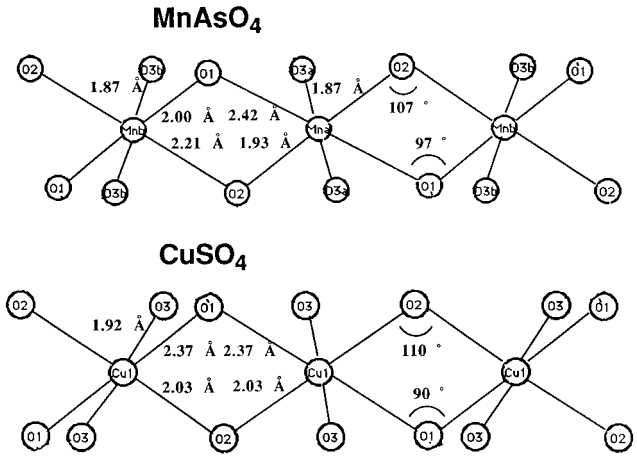

Figure 7. Schematic views of the edge-sharing MO_6 chains for (a) $MnAsO_4$ and (b) $CuSO_4$ with some bond distances and angles labeled.

the crystallographically inequivalent Mn(a) and Mn(b) positions are related by a simple $a/2$ translation. This is an interesting example of a crystallographically indeterminate problem.

The antiferromagnetic order is commensurate with a $2a \times b \times 2c$ supercell in which eight Mn(a) (or Mn(b)) spins are ordered but the other eight Mn(b) (or Mn(a)) spins are disordered. Such a disordered sublattice within a magnetically ordered material is known as "idle" spin behavior. This has previously been reported in β-$LiMnFeF_6$,[18] in which the Fe^{3+} sublattice orders at a higher temperature than the Mn^{2+} spins, reflecting the relative strength of their superexchange interactions. $MnAsO_4$ is notable in having Mn^{3+} spins in similar chemical environments as both the ordered and disordered components. Furthermore, there is no evidence for a transition to a fully ordered magnetic structure down to 1.6 K.

The unusual magnetic phase of $MnAsO_4$ below the simultaneous Neel and spin-glass transition results from frustration of the magnetic exchange pathways. The observed magnetic structure is consistent with dominant antiferromagnetic superexchange interactions between spins in one sublattice with each other as discussed below. The spins in the other sublattice are coupled to equal numbers of "up" and "down" spins in the ordered sublattice, and so the interactions are frustrated and no long-range order of this sublattice occurs. However, local

(18) Courbion, G.; De Pape, R.; Teillet, J.; Varret, F.; Pannetier, J. *J. Magn. Magn. Mater.* **1984**, *42*, 217.

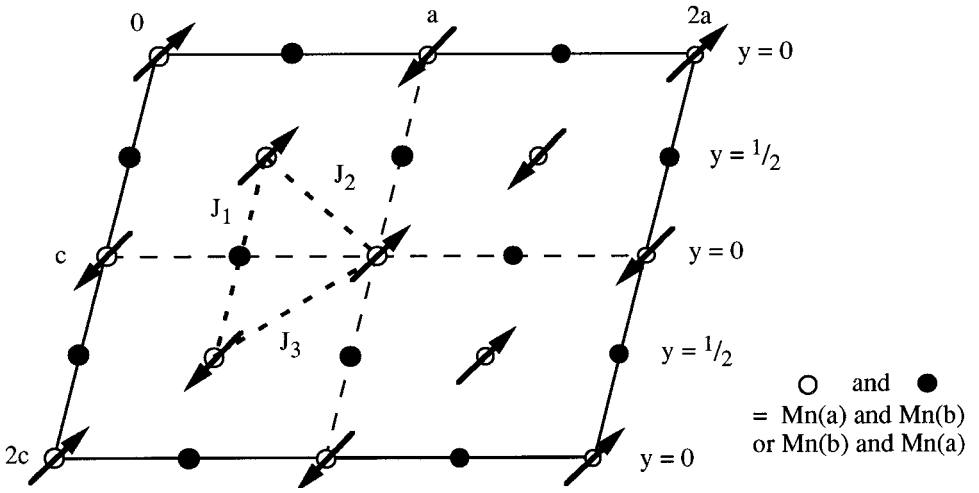

Figure 8. Schematic exchange interactions between spins in magnetically ordered $MnAsO_4$. The three inequivalent interactions, mediated by the Mn−O−As−O−Mn bridges, are outlined.

coupling of the disordered spins to the ordered neighbors reduces their relaxation rates so that they show some characteristics of a spin glass, in having divergent zero-field-cooled and field-cooled susceptibilities, although this is not evidenced in the ac measurements. Further work is needed to understand the magnetic behavior of the disordered spins below 14.5 K and to determine whether the 4.5 K anomaly in χ' is a spin-glass transition. Coupling to the disordered spins will give rise to local reorientations of the ordered spins leading to a reduced value of the ordered saturation moment. The observed value of 2.6 μ_B is considerably less than the values of ≈3.5 μ_B (reduced from the ideal value of 4.0 μ_B by zero-point motion and Mn−O covalency) usually found for high-spin manganese(III) in phosphates and arsenates.[7−9] The exponent deduced from the fit shown in Figure 4, 0.20, is not strictly the exponent that describes the critical behavior of this compound as there are not enough experimental data close to the critical temperature.

Although $MnAsO_4$ and $CuSO_4$ both contain Jahn−Teller-distorted octahedra, their cooperative distortions and magnetic structures are different. Figure 7 displays the edge-sharing chains of MO_6 octahedra in both structures. In the $CuSO_4$ structure each bridging oxygen forms either two short or two long bonds to the Cu^{2+} ions. This symmetric bridge allows lobes of the same orbital type to overlap with the common bridging oxygen. For Cu^{2+} the "magnetic" (half-filled) $d_{x^2-y^2}$ orbitals are associated with the short Cu−O bonds (Figure 7b) which interact through the bridging angle of 110° to give a strong antiferromagnetic intrachain interaction. However, the cooperative Jahn−Teller distortion in $MnAsO_4$ results in an asymmetric bridge (Figure 7a) in which each bridging atom involves a half-filled d_{z^2} orbital and an empty $d_{x^2-y^2}$ lobe, and so is very weak. π-superexchange interactions involving the t_{2g} type orbitals are also weak due to the elongated Mn−O bonds in each bridge. Hence, the intrachain Mn···Mn superexchange in $MnAsO_4$ is weak, and the magnetic structure is determined by interchain Mn−O−As−O−Mn interactions.

Each Mn spin is linked to those in neighboring chains by several inequivalent Mn−O−As−O−Mn linkages, which give rise to antiferromagnetic couplings between the spins. The observed magnetic structure of $MnAsO_4$ suggests that the interactions between spins in one of the sublattices are stronger than those in the other or those between the Mn(a) and Mn(b) sublattices. Figure 8 shows the exchange interactions between spins in the magnetically ordered sublattice mediated by Mn−O−As−O−Mn bridges. Three inequivalent interactions occur in a triangular network, and the observed magnetic structure is consistent with $|J_1|, |J_3| \gg |J_2|$ so that the latter interactions are completely frustrated. In the orthorhombic $CuSO_4$ type parent structure the J_2 and J_3 interactions are equivalent, but the monoclinic distortion of the structure due to Jahn−Teller effects evidently changes the magnitude of these interactions significantly. Explanation in terms of the geometries of the Mn−O−As−O−Mn pathways involved is not possible as we do not know which of the two Mn sites is magnetically ordered.

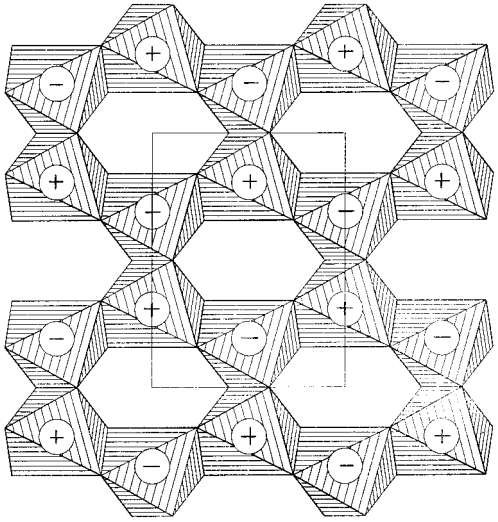

Figure 9. (001) view of a layer of linked MnO_6 octahedra in $Mn_2As_2O_7$ showing the magnetic ordering and the unit cell.

$Mn_2As_2O_7$. The high-temperature effective moment (Table 1) for manganese(II) pyroarsenate is typical for high-spin d^5 Mn^{2+}, and the negative Weiss Θ constant indicates that weak antiferromagnetic interactions occur between spins. The magnetic transition observed at 10.5(5) K (Figure 1) is typical of long-range antiferromagnetic ordering.

$Mn_2As_2O_7$ adopts a thorveitite type structure[19] in which each MnO_6 octahedron shares three edges with other octahedra to give layers in the *ab* plane. Antiferromagnetic Mn−O−Mn interactions through the shared edges, in accordance with Goodenough−Kanamori rules,[20] result in a simple nonfrustrated

(19) Cruickshank, D. W. J.; Lynton, H.; Barclay, G. A. *Acta Crystallogr.* **1962**, *15*, 491.

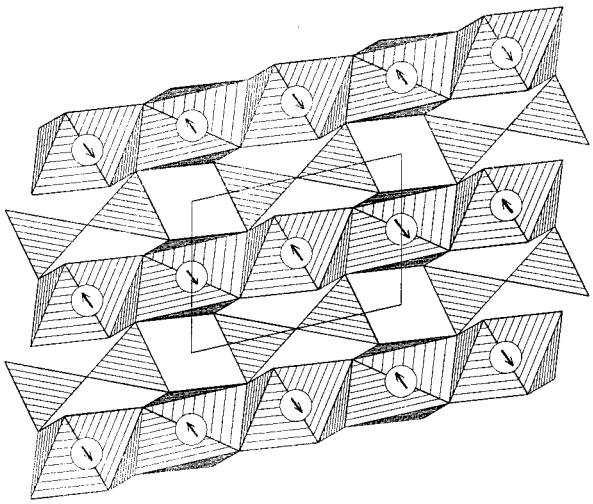

Figure 10. Packing of the Mn−O layers along the *c* axis for $Mn_2As_2O_7$, with the magnetic structure and the fundamental unit cell shown.

spin arrangment (Figure 9). These layers are stacked along the *c* axis, with pyroarsenate groups between the layers (Figure 10). Weak antiferromagnetic interlayer interactions through Mn−O−As−O−Mn pathways couple each layer antiferromagnetically to the next, resulting in the doubled magnetic *c* parameter. The magnetic moments are aligned in the *ac* plane pointing 29° from the *c* axis, and the value of 4.2 μ_B at 1.6 K is typical for such a nonfrustrated system, with a reduction from 5.0 μ_B due to covalency.

During the course of this work, the magnetic structures of $M_2As_2O_7$ compounds (M = Mn, Ni, Co) were independently studied by Buckley and co-workers[21] by using low-temperature constant-wavelength neutron data. These authors could not fully refine the magnetic structure of $Mn_2As_2O_7$; however, with the same model as we have reported and magnetic components $\mu_x = 2.34\ \mu_B$ and $\mu_z = 4.42\ \mu_B$, they found a good agreement between the observed and calculated intensities of the principal magnetic peaks. Our refined values of $\mu_x = 1.1(2)\ \mu_B$ and $\mu_z = 4.1(1)\ \mu_B$ are in remarkably good agreement as this phase constitutes only 20% of our sample and show that good-quality multiphase refinements of crystal and magnetic structures are possible with high-resolution neutron diffraction data.

Acknowledgment. We thank Drs. R. B.Von Dreele (MLNSC) and R. M. Ibberson (RAL) for assistence with the collection of neutron data. MLNSC, Los Alamos National Laboratory, is operated under U.S. Government Contract W-7405-ENG-36, and neutron facilities at RAL were provided by the EPSRC. The work in Malaga (Spain) and Cambridge (U.K.) was supported by Research Grants CICYT PB93/1245 and EPSRC GR/K75040, respectively.

Supporting Information Available: Tables S1 and S2, giving full details of the HIPD neutron refinements at 15 and 11 K and of the HRPD neutron refinements at 5 and 1.6 K, Tables S3−S5, listing refined atomic parameters for $MnAsO_4$ at 11, 5, and 1.6 K, respectively, Tables S6−S8, listing refined atomic parameters for $Mn_2As_2O_7$ at 11, 5, and 1.6 K, respectively, and Table S9, giving bond distances and angles for $Mn_2As_2O_7$ at 15 K (6 pages). Ordering information is given on any current masthead page.

IC970858Y

(20) Goodenough, J. B. *Magnetism and the chemical bond*; Wiley: New York, 1963.

(21) Buckley, A. M.; Bramwell, S. T.; Day, P.; Visser. D. *J. Solid State Chem.* **1995**, *115*, 229.